Supplementary information

Dynamic nature of disulfide bond formation catalysts revealed by crystal structures of DsbB

Kenji Inaba*, Satoshi Murakami, Atsushi Nakagawa, Hiroka Iida, Mai Kinjo, Koreaki Ito and Mamoru Suzuki

Legends to supplementary figures

Fig. S1. Two Reaction Pathways in DsbB-Catalyzed DsbA Oxidation.

The rapid pathway proceeds through sequential dithiol/disulfide exchanges between the active site cysteines, while the slow pathway proceeds through the more concerted action of DsbB cysteines before releasing oxidized DsbA from the DsbB-DsbA complex. The commitment steps for the two pathways are supposed to be in the nucleophilic attacks (shown by red arrows) by Cys33 of DsbA (rapid pathway) and by Cys130 of DsbB (slow pathway) of the respective target cysteines (DsbA Cys30 and DsbB Cys41, respectively), as described in our previous paper (Inaba et al, 2005). During these processes, DsbB-bound UQ undergoes the electronic transition ascribed to the Cys44-UQ CT complex formation (Inaba et al, 2006b) as shown by color change of UQ. This figure originated from Inaba et al. (2005) but is slightly modified based on the content of this paper.

Fig. S2 Anomalous scattering peaks from SeMet-labeled DsbB derivatives

Bijvoet anomalous difference-Fourier maps of SeMet-labeled wild-type, V120M and C130M DsbB derivatives, which were used for coordinate building of the original DsbB-DsbA complex structure (Inaba et al, 2006a). The anomalous scattering peaks of selenium atoms

contoured at 3.0σ are shown in blue. The positions of selenium signals that appeared upon V120M and C130M mutations are shown by red asterisks with residue numbers in the right two panels.

Fig. S3 Catalytic DsbA oxidation by membrane-embedded DsbB variants having mutations in the horizontal helix region.

Membrane fractions were prepared from cells overproducing indicated DsbB variants, as described previously (Bader et al, 1998). 10 μM of reduced DsbA was reacted with the membrane at 30 °C in 50 mM Tris, pH8.1, 0.1 M NaCl, in which concentrations of membrane-integrated DsbB proteins were unified to 100 nM. The reaction was quenched by the addition of final 5 % of TCA at the indicated times. Samples were then subjected to pellet-down, acetone wash, AMS modification and SDS-PAGE (12.5 %). Redox state of DsbA was visualized by CBB staining. Whereas Ala-substitutions for Leu114 and Leu116 and Leu-substitutions for Val120, Val123 and Phe124 did not affect DsbA oxidation activity of DsbB, the other mutations grossly impaired the functionality of DsbB.

Fig. S4 DTT resistance of membrane-embedded DsbB variants with mutations in the horizontal helix region

The indicated membrane-embedded DsbB derivatives were incubated with indicated concentrations of DTT in 50 mM Tris, pH8.1, 0.1 M NaCl at 30 °C for 30 min. Samples were subsequently TCA-precipitated and processed for AMS modification. Redox states of DsbB were monitored by Western blot analysis (12.5 %) with anti-myc antibody. DsbB(ΔY46) is a control that is defective in the functional redox interaction with UQ and therefore not

refractory to reduction with DTT (Kobayashi et al, 2001). Mutations in the horizontal helix regions did not affect DTT resistance of membrane-embedded DsbB.

Fig. S5 Stoichiometric redox reactions between DsbA and quinone-free DsbB

Disulfide exchange reactions between reduced DsbA and the quinone-free form of DsbB variants were investigated *in vitro* by essentially the same method as described previously (Inaba et al, 2005). Briefly, equimolar amounts (10 μM) of DsbA and indicated DsbB derivatives were incubated at 30 °C for the indicated time in fully degassed buffer containing 50 mM Tris-HCl, pH8.1, 0.1 M NaCl and 0.02 % N-dodecyl-β-D-maltoside. After reaction, samples were TCA-precipitated, AMS-modified and visualized by CBB staining on SDS-PAGE (12.5 %). Whereas wild-type DsbB oxidized ~40 % of reduced DsbA without the aid of ubiquinone, the mutant with Asp- or Pro-substitutions for Leu114 and Leu116 lost the ability to accept electrons from DsbA.

Supplemental References

Bader M, Muse W, Zander T, Bardwell J (1998) Reconstitution of a protein disulfide catalytic system. *J Biol Chem* **273:** 10302 - 10307

Inaba K, Murakami S, Suzuki M, Nakagawa A, Yamashita E, Okada K, Ito K (2006a) Crystal structure of the DsbB-DsbA complex reveals a mechanism of disulfide bond generation. *Cell* **127:** 789 - 801

Inaba K, Takahashi YH, Ito K (2005) Reactivities of quinone-free DsbB from Escherichia coli. *J Biol Chem* **280:** 33035 - 33044

Inaba K, Takahashi YH, Ito K, Hayashi S (2006b) Critical role of a thiolate-quinone charge transfer complex and its adduct form in de novo disulfide bond generation by DsbB. *Proc Natl Acad Sci U S A* **103:** 287 - 292

Kobayashi T, Takahashi Y, Ito K (2001) Identification of a segment of DsbB essential for its respiration-coupled oxidation. *Mol Microbiol* **39:** 158 - 165

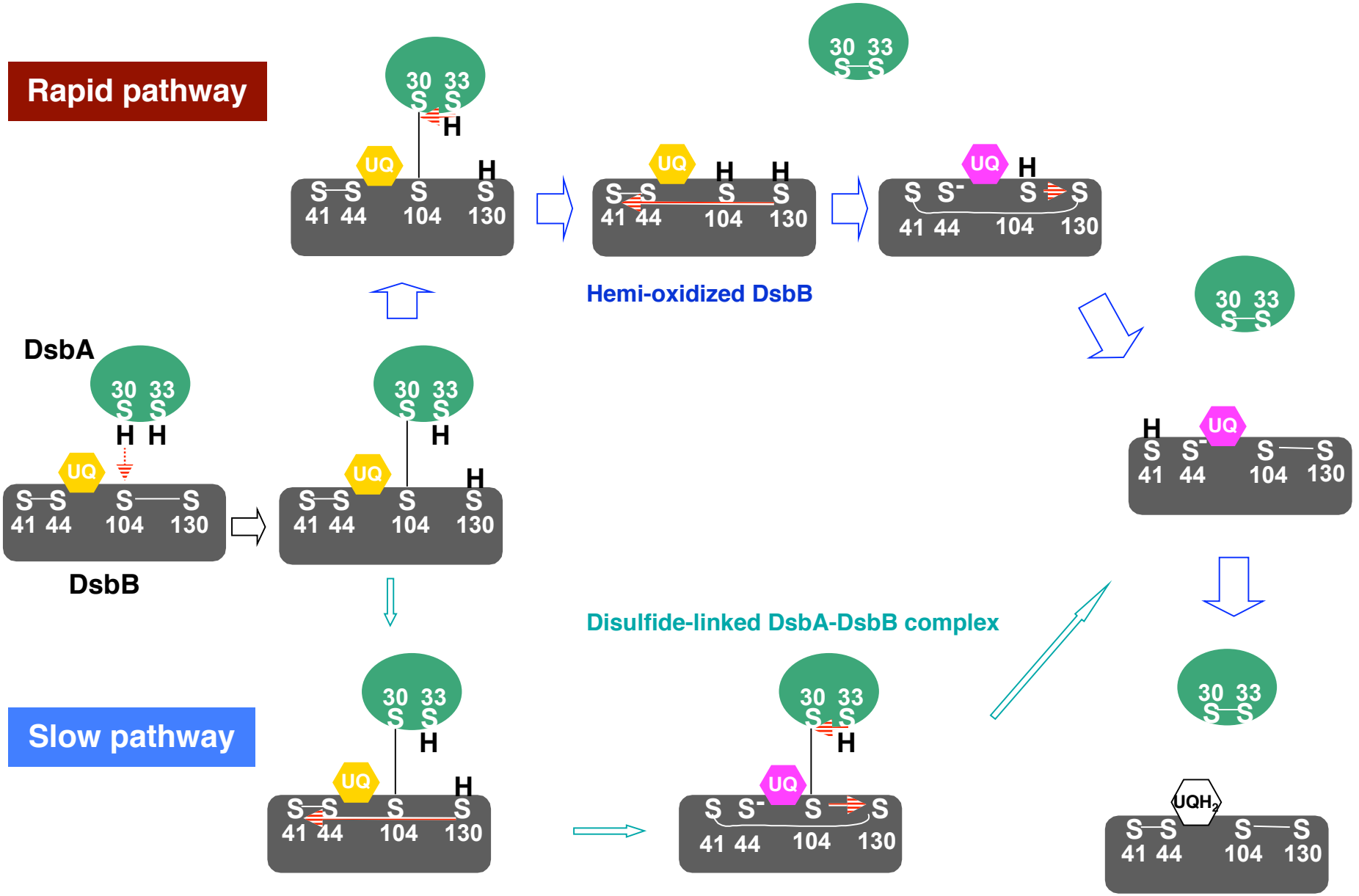

Supplementary Fig. S1 Inaba et al.

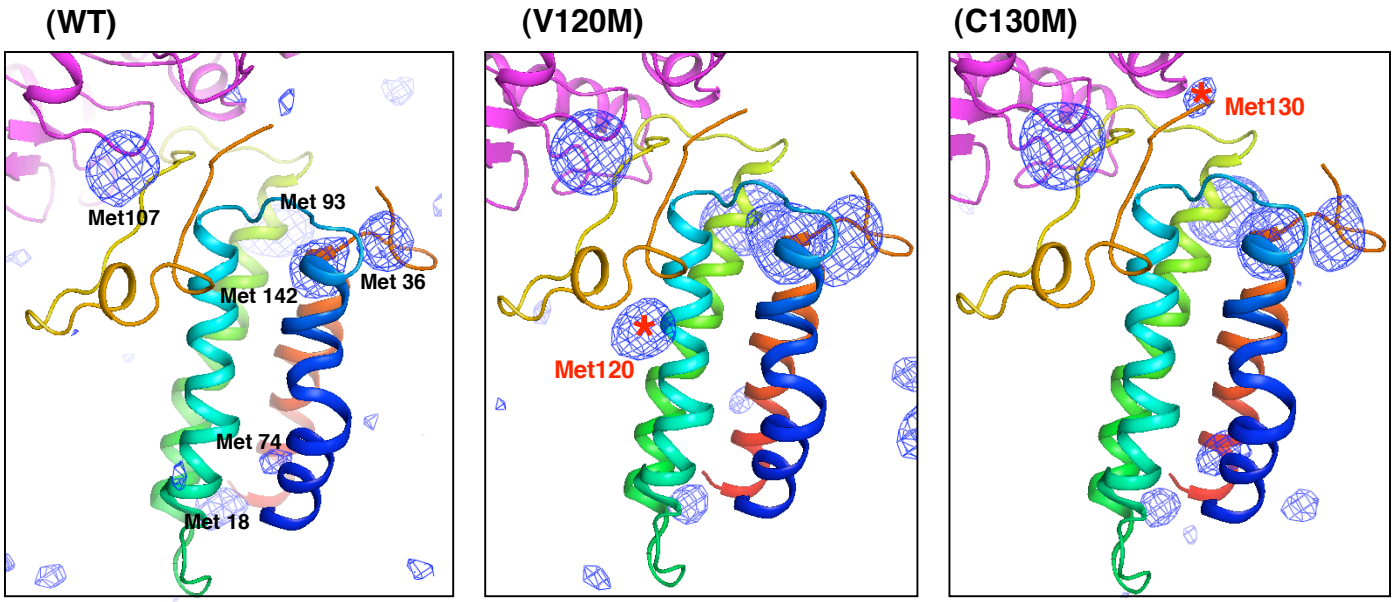

Supplementary Fig. S2 Inaba et al.

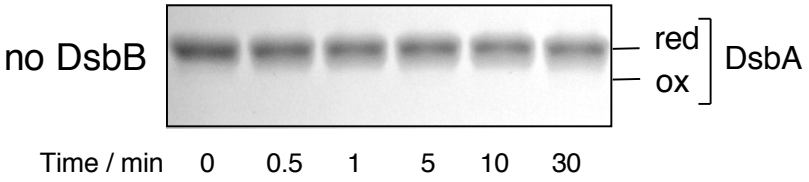

(Mutations at Leu114 & Leu116)

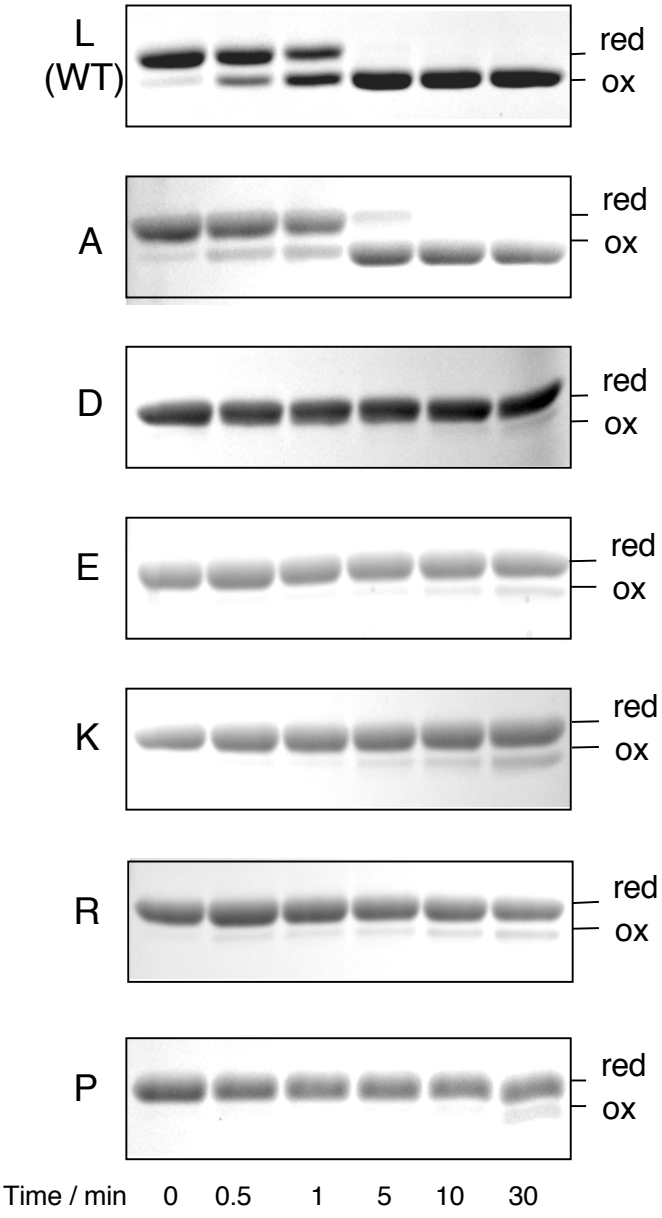

(Mutations at Leu114 , Leu116, Val120, Val123, Phe124)

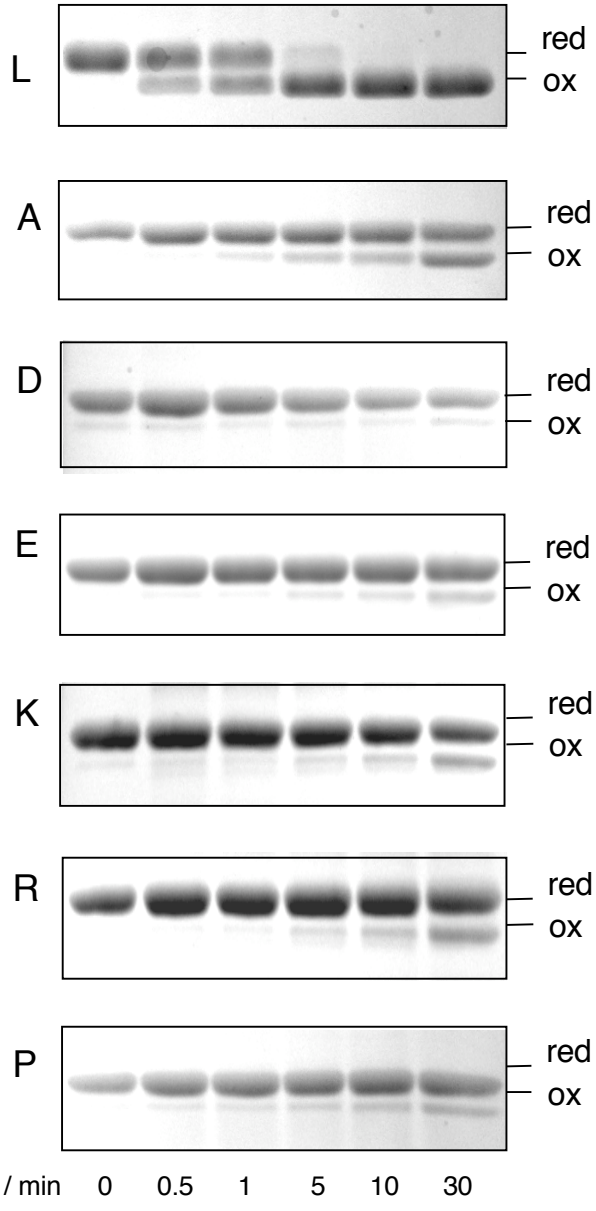

Supplementary Fig. S3 Inaba et al.

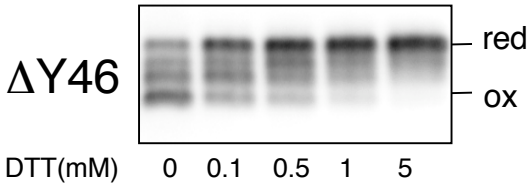

(Mutations at Leu114 & Leu116)

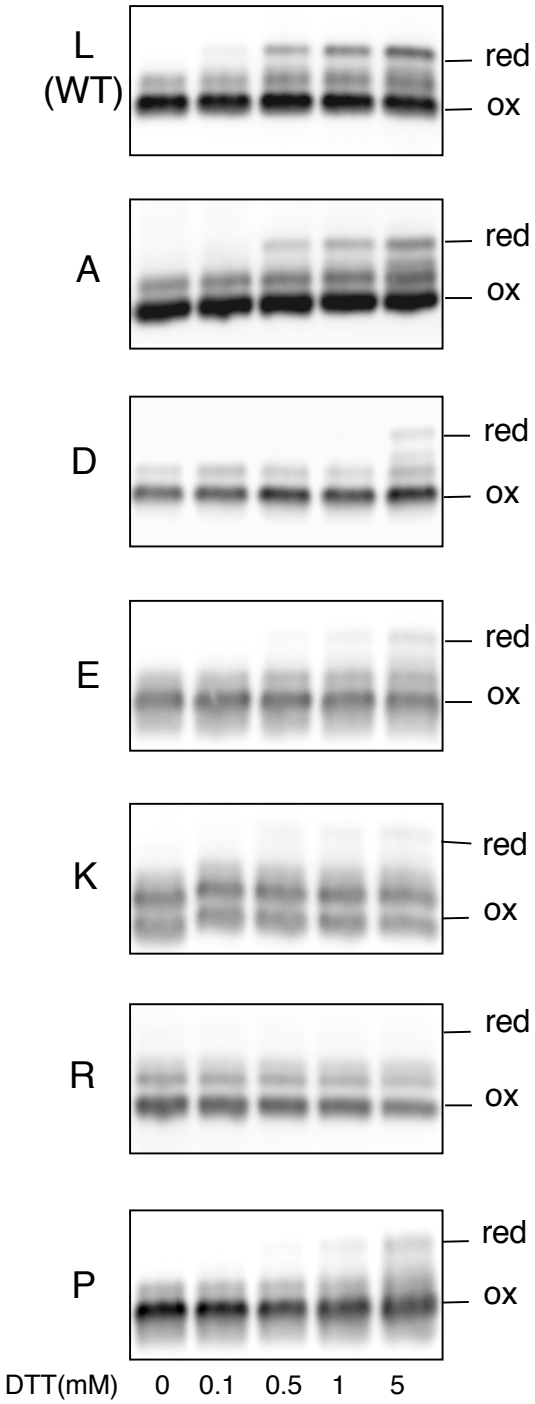

(Mutations at Leu114 , Leu116, Val120, Val123, Phe124)

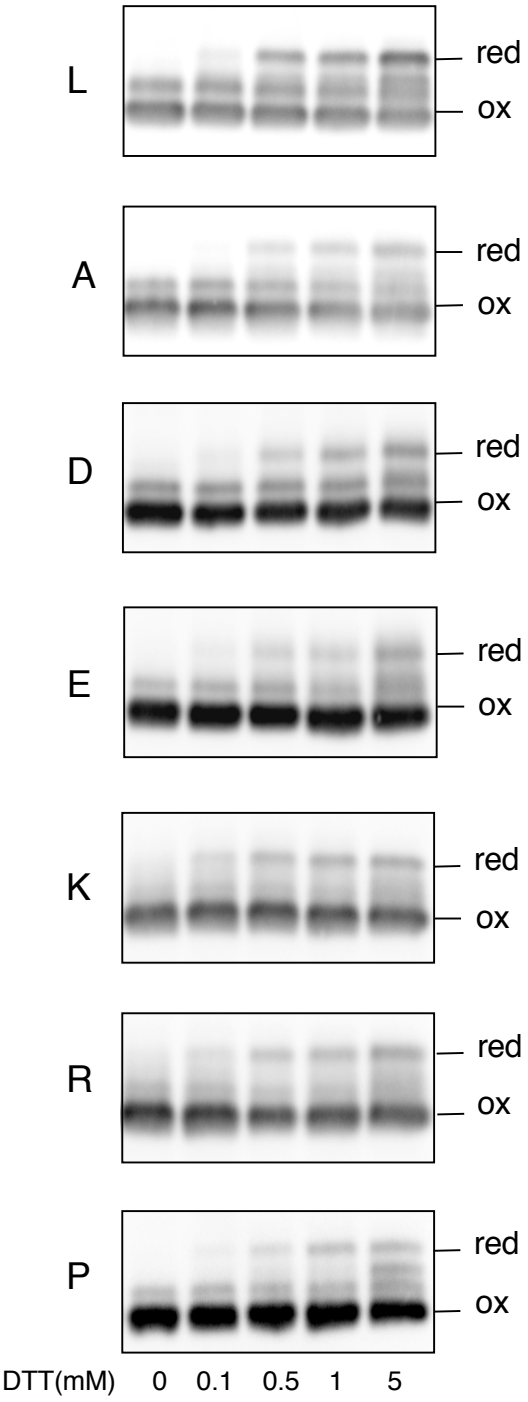

Supplementary Fig. S4 Inaba et al.

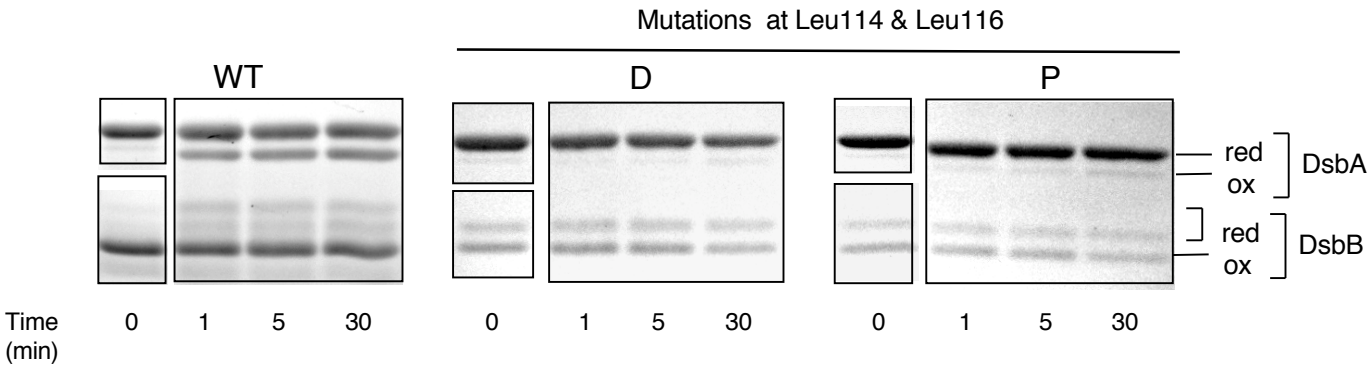

Supplementary Fig. S5 Inaba et al.

Supplementary Table SI. Data collection and crystallographic analysis for the methionine-marking method

	DsbB L114M	DsbB V123M	DsbB S127M	DsbB L138M
Beamline	BL44XU at SPring-8	BL44XU at SPring-8	BL44XU at SPring-8	BL44XU at SPring-8
Space group	*C*2	*C*2	$P4_22_12$	*C2*
Cell dimensions (Å)	*a* = 128.1, *b* =108.9, *c* = 66.5	*a* = 127.2, *b* =105.9, *c* = 65.6	*a* = *b* = 167.2, *c* = 66.1	*a* = 127.7, b=107.7, *c* = 65.7
	(β = 90.4 °)	(β = 90.6 °)		(β = 90.3 °)
Wavelength (Å)	0.97858	0.97887	0.97882	0.97887
Resolution (Å)	46.0 – 4.2 (4.4 – 4.2)	20.1 – 4.0 (4.2 - 4.0)	49.5 – 7.0 (7.4 – 7.0)	19.9 – 4.0 (4.2 – 4.0)
No. of total observations	19,823 (1,785)	25,467 (2,781)	19,892 (3,030)	23,536 (2,172)
No. of unique reflection	6,137 (732)	7,127 (891)	1,663 (242)	6,085 (758)
$I / \sigma(I)$	10.5 (3.0)	14.0 (3.8)	22.2 (8.7)	9.2 (2.5)
Completeness (%)	92.7 (76.3)	96.0 (82.0)	99.4 (99.8)	95.1 (81.1)
Multiplicity	3.2 (2.4)	3.6 (3.1)	12.0 (12.5)	3.5 (2.9)
R_{merge}[a]	0.085 (0.431)	0.052 (0.345)	0.085 (0.367)	0.076 (0.380)

Numbers in parentheses represent statistics in the highest resolution shell.

[a] $R_{merge} = \Sigma\Sigma_j|\langle I(h)\rangle - I(h)_j| / \Sigma\Sigma_j|\langle I(h)\rangle|$, where $\langle I(h)\rangle$ is the mean intensity of symmetry-equivalent reflections.